

Measuring Sulfur Content and Corrosivity of North American Petroleum with the Advanced Distillation Curve Method

Peter Y. Hsieh and Thomas J. Bruno*

Material Measurement Laboratory, Applied Chemicals and Materials Division, National Institute of Standards and Technology, 325 Broadway, MS 647.07, Boulder, Colorado 80305, United States

S Supporting Information

ABSTRACT: Petroleum is a complex fluid whose sulfur content varies considerably depending on its place of origin. Sour crude petroleum, which contains more than 0.5% sulfur by mass, often requires additional processing due to the potential for corrosion and catalyst poisoning during refining. Estimating or measuring the sulfur content of distillate fractions as a function of boiling temperature is an important step in petroleum refining. The advanced distillation curve (ADC) method was developed to provide a composition-explicit data channel for the measurement of thermophysical and chemical properties of complex fluids. We applied the ADC method to a composite sample of North American petroleum to characterize its boiling temperature, density, and composition as a function of distillate volume fraction. The compositions of light distillate fractions were used to estimate their densities and refractive indices based on critically evaluated thermodynamic data. The estimated densities of the distillate fractions are consistent with pycnometry data. The sulfur content, measured with a sulfur chemiluminescence detector, was found to be within the range predicted by an empirical model based on distillate boiling temperature and density. The corrosivity of various distillate cuts was tested with a modified copper strip corrosion test. Copper tarnishing was found to depend not only on the amount of sulfur present but also on the temperature at which the fraction is collected.

1. INTRODUCTION

Petroleum, or crude oil, is a valuable commodity because it is the feedstock for a wide range of products from fuels to plastics. The formation of petroleum from fossilized remains of phytoplankton is a complex geological process. The complexity of the process adds considerable variability to petroleum composition across the world. Crude oils contain thousands of components, each with different thermophysical and chemical properties. Petroleomics, or the prediction of crude oil properties by identifying and characterizing all compounds present in the complex fluid, is becoming an increasingly significant tool in petroleum production and refining.^{1,2} In particular, petroleomics can improve the estimation of sulfur content in crude oil, which is a significant issue in petroleum refining.

Sulfur is a common impurity in petroleum. Crude oils containing relatively few sulfur impurities are referred to as “sweet”; they are considered “sour” if they contain more than 0.5% sulfur by mass. Sour crude oils derived from unconventional sources, such as tar sands, are becoming more important as the world supply of “sweet” crude oil dwindles. Because of their high sulfur content, they are more difficult to refine into motor fuels. Sulfur in the fuel can poison catalysts used in emission control systems. For this reason, ultralow sulfur diesel (ULSD) fuel sold in North America must contain less than 15 ppm (ppm) sulfur;³ in Europe, the sulfur content limit is even lower, at 10 ppm.^{4,5} Similar sulfur content limits are being adopted by other parts of the world to reduce air pollution. In addition, sulfur also deactivates catalysts used during petroleum refining to crack large hydrocarbon molecules into the smaller ones found in gasoline and diesel fuel.⁶ Catalyst deactivation lowers the overall yield of motor fuels obtainable through

hydrocracking during refining. Sulfur removal is an important step in petroleum refining.

The measured or estimated sulfur content of crude oil and its distillate fractions is an important factor in determining the capital and operating costs of hydrodesulfurization processing units in a petroleum refinery.⁷ In a petroleum refinery, crude oil is fractionated or separated into its components through distillation. Distillation separates the compounds that comprise petroleum by their boiling temperatures into distillate fractions or cuts. Each distillate cut contains a different blend of sulfur compounds. Sulfur compounds can be nonrefractory or refractory. Sulfur can be readily removed from nonrefractory sulfur compounds through hydrodesulfurization, a process whereby sulfur compounds are converted to hydrogen sulfide gas in the presence of catalysts and hydrogen gas.⁸ Refractory sulfur compounds, such as alkyl benzothiophenes and dibenzothiophenes, are less reactive, and the sulfur present in these compounds is difficult to remove during petroleum refining.⁹ The size of the hydrodesulfurization processing unit needed to treat a given distillate fraction depends on the amount and type of sulfur compounds it contains. Removal of refractory sulfur compounds is currently an active area of research.

The quantitative analysis of sulfur in crude oil and distillate fractions thereof has received considerable attention for over a century. Early measurements relied on wet chemistry assays, where the sample is first burned in an oxygen bomb calorimeter¹⁰ and the amount of sulfur measured through

Received: December 17, 2013

Revised: February 4, 2014

Published: February 5, 2014

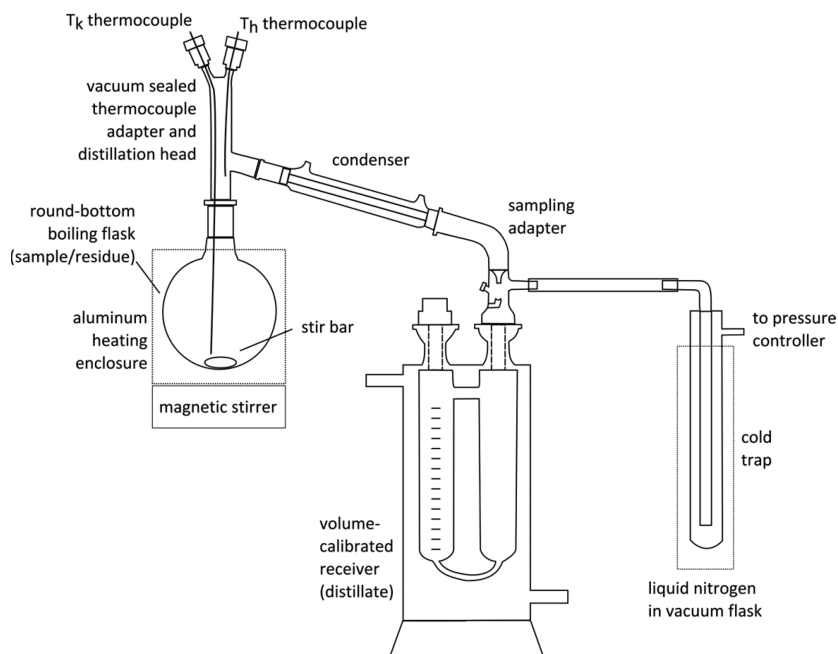


Figure 1. Schematic diagram of reduced pressure ADC apparatus. To better illustrate important features, the components shown are not to scale.

acid–base titration¹¹ or by weighing the barium sulfate formed in a precipitation reaction.¹² Electrochemical analyses, such as polarographic measurement of free sulfur in solution¹³ and gas chromatography with coulometric detection,¹⁴ have improved the throughput and sensitivity of sulfur testing in the laboratory. Further improvements have been made through optical measurement methods, including photometric measurement of lead acetate darkening in the presence of hydrogen sulfide gas¹⁵ and chemiluminescence flame-emission measurements based on sulfur dioxide concentration.¹⁶ The chemiluminescent reaction between ozone and sulfur monoxide generated from combustion of sulfur compounds in petroleum fractions is the basis for the modern sulfur chemiluminescence detector (SCD).^{17,18} The measurement of sulfur content in unconventional petroleum, such as synthetic crude derived from oil sands, remains challenging due to the large size of the asphaltene molecules present. X-ray based methods have been investigated to quantify sulfur in heavy petroleum fractions.^{19–21}

Sample handling and storage are important considerations in the measurement of sulfur content in petroleum samples. Hydrogen sulfide gas has a high vapor pressure at ambient temperature and readily escapes from an unconfined sample. Small organosulfur molecules, such as thiols, adsorb readily onto uncoated glass and metal surfaces. Loss of sulfur compounds through evaporation or adsorption can decrease the measured sulfur content. Riazi et al. proposed an empirical correlative model using the boiling temperatures and densities of pseudocomponents obtained through distillation to predict the sulfur content of crude oils and reservoir fluids.²² Measurements of these thermophysical properties are common laboratory procedures for analysis of crude oil.^{23–25} An indirect estimate of sulfur content based on routinely collected data may be a useful tool in complementing direct measurements of sulfur content or as a substitute when a direct measurement is not possible.

The Advanced Distillation Curve (ADC) is a significant improvement over earlier discrete approaches to complex fluid

characterization, featuring (1) a composition-explicit data channel for each distillate fraction (for both qualitative and quantitative analysis), (2) temperature measurements that are true thermodynamic state points that can be modeled with an equation of state, (3) temperature, volume, and pressure measurements of low uncertainty suitable for development of equations of state, (4) consistency with a century of historical data, (5) an assessment of the energy content of each distillate fraction, (6) trace chemical analysis of each distillate fraction, and (7) a corrosivity assessment of each distillate fraction.^{26–28} It has been used to characterize *n*-alkanes,²⁹ simple azeotropes,³⁰ gas turbine fuels,^{31–36} diesel and biodiesel fuels,^{37–42} gasolines,^{43–45} rocket propellants,^{31,46–48} and crude oils.^{49–52} Unlike the conventional distillation curve, fuel volatility or vapor–liquid equilibrium data, ADC data can be modeled by an equation of state.^{53–58}

In this paper, we show how ADC thermophysical and composition data can be used with the Riazi correlation model to estimate the sulfur content of crude oil. The results can be compared directly with SCD data from the corresponding distillate fractions or cuts. In addition, the corrosivity of the distillate as a function of sulfur content can be tested by measuring the degree to which copper coupons are tarnished when immersed in a diluted aliquot of the distillate.^{49,50,52} Earlier work by Andersen et al. suggests that the sulfur content alone is insufficient in determining whether a hydrocarbon sample will be corrosive.⁵⁹ The distillation of sour crude petroleum at atmospheric and reduced pressure yields fractions with varying sulfur content obtained at different temperatures, which is useful in testing the effect of temperature as well as sulfur content on corrosivity. Sulfur-induced corrosion of metals is a significant reason for measuring sulfur content in crude oil, distillate, and residual fractions. Corrosion resistant alloys, such as carbon steel, stainless steel, and nickel-based alloys, are often employed in the construction of refineries.⁶⁰ Characterization of the conditions necessary for the production of corrosive sulfur compounds is important in minimizing

sulfur-induced corrosion during refining, storage, and use of petroleum products.

2. MATERIALS AND METHODS

A composite sample of North American petroleum was obtained from a refinery in Cheyenne, Wyoming, USA.⁶¹ The *n*-tetradecane solvent was purchased from a commercial supplier and determined to be approximately 99% (mass/mass) pure through gas chromatography with mass spectrometric detection. Trace quantities of toluene and *n*-dodecane were found to be present in the solvent. The contaminant peak areas were largely consistent between measurements, and their contributions were removed during data analysis by subtracting the background signal from the solvent. The *n*-hexane solvent used was purchased from a commercial supplier and determined to be approximately 99% (mass/mass) pure through gas chromatography with flame-ionization detection. No significant contaminant peaks were observed in the *n*-hexane. The solvents were used without further purification.

2.1. Advanced Distillation Curve Apparatus and Method.

The reduced pressure ADC apparatus and sampling method have been described in greater detail in earlier works, with applications reported for biodiesel fuels,^{62,63} crude oils, and waste oils.⁶⁴ Unlike the open apparatus specified in the ASTM D-86 atmospheric distillation method and the atmospheric pressure ADC method, the reduced pressure ADC apparatus (Figure 1) constitutes a closed system for mass transfer. The apparatus is conceptually similar to the atmospheric pressure ADC apparatus, but it has provisions for controlled low pressure operation and vacuum tight seals around the feedthroughs in the thermocouple adapter. The fluid sample inside the boiling flask was mixed by a magnetically driven stir bar. The aluminum heating enclosure around the boiling flask, along with stirring, ensures uniform heating of the sample. Prior distillation data were consulted to establish a temperature ramp rate that produced a steady mass transfer rate at the condenser. Distillations were stopped below 400 °C to minimize hydrocarbon cracking and to maintain a greater margin of safety for working with borosilicate glass under reduced pressure. As an additional precaution to counteract bumping, or localized superheating and rapid boiling, a shard of glass (approximately 1 g) was added to the boiling flask prior to distillation. The sharp edges and corners on the glass shard add nucleation sites to prevent bumping during distillation.

The vacuum sealed thermocouple adapter and distillation head link the boiling flask to the condenser and provide access for two thermally tempered 1.6 mm diameter K-type thermocouples sheathed in stainless steel. A silicone O-ring surrounding the thermocouples inside of a compression fitting threaded into the top of the distillation head creates a vacuum tight seal around the inserted thermocouples. The thermocouples are inserted into the distillation head and the boiling flask to monitor the vapor temperature at the bottom of the distillate takeoff position (T_h) and the liquid temperature in the boiling flask (T_k).

From the distillation head, the distillate vapor flows into an air-cooled condenser. The distillate liquid formed therein enters a sampling adapter that allows for instantaneous sampling of the distillate. The position of the sampling adapter is shown in Figure 1. The distillate fluid is directed into a 0.05 mL "hammock" from which an aliquot of the distillate was drawn using a standard chromatography syringe at ambient pressure or a pressure-balanced syringe at reduced pressure. Typical aliquots range between 5 and 25 μ L in volume. This volume is adequate for most analyses and will introduce no unacceptable uncertainty into the volume measurements.

When the distillate sample leaves the sampling adapter, it drips into the calibrated receiver for precise volume measurement. The receiver used in the reduced pressure ADC apparatus is similar to atmospheric pressure receivers, except for the addition of a ground glass ball joint connection. The ball joint connection, sealed with high vacuum grease and a pinch clamp, provides flexibility in the angle between the adapter and the receiver. The receiver consists of two cylinders of equal diameter with calibrated volume markings; the volume was calibrated

from 0 to 100 mL in 1 mL increments with a volumetric pipet. The distillate volume was measured throughout the distillation using the calibrated volume markings.

Due to petroleum's opacity and viscosity, the initial sample volume in the boiling flask was determined through its mass and density. The boiling flask was placed on a cork ring atop a triple-beam balance, and filled slowly with petroleum from a beaker until the mass reached a predetermined value. Distillate volume fraction was calculated by dividing the distillate volume by the initial sample volume. The uncertainty estimates of the three measured values (sample mass, density, and distillate volume) were combined in quadrature to determine the uncertainty of the distillate volume fraction.

A commercial proportional, integral, derivative (PID) vacuum controller was connected to the sampling adapter vacuum port to measure and control the system pressure. The controller uses a piezoresistive pressure transducer and continuously regulated proportional valves for evacuation and venting to control the reduced pressure. The pressure controller can maintain a set pressure between 1 to 83 kPa (0.1 kPa resolution, 0.1 kPa estimated uncertainty). The pressure transducer was calibrated by measuring the vapor pressure of deionized water as a function of temperature (see the Supporting Information, section S1, for additional details). A liquid nitrogen cold trap was placed between the apparatus and the pressure controller to condense any vapors that might escape the apparatus. The sum of recovered liquid volumes in the boiling flask (kettle), calibrated receiver, and cold trap was typically within 1% of the initial sample volume.

A gas reservoir containing 1 L of carbon dioxide was connected directly to the vacuum controller as a safety measure during reduced pressure distillations. The volume of the carbon dioxide gas in the reservoir exceeds the total system volume of the ADC apparatus. If the system must be brought to atmospheric pressure quickly, the carbon dioxide from the reservoir prevents air from coming into contact with the hot hydrocarbon liquid in the boiling flask. The risk of fire during atmospheric pressure distillation is minimal, as a similar blanketing process occurs when hydrocarbon vapor from the boiling sample displaces air within the ADC apparatus at the start of the distillation. The cool hydrocarbon vapor in the condenser prevents air from entering the boiling flask and coming into contact with the hot petroleum sample.

Due to the large differences in vapor pressures of the compounds that make up the sample, two methods have been developed for measuring the distillation curve at reduced pressure (1 kPa or 0.01 atm). In the first approach, the petroleum was frozen in liquid nitrogen prior to the start of distillation. Unlike typical reduced pressure ADC measurements, the distillation was not started at ambient temperature; instead, it was started at a sample temperature (T_k) of -100 °C. For these measurements, the sample was frozen after the thermocouples were in place and the distillation head was attached to the boiling flask. The light distillate fractions, which boil below room temperature at reduced pressure, can be recovered from the cold trap at ambient temperature and pressure. In the second approach, the sample was first distilled at ambient pressure to measure the boiling temperatures of light distillate fractions. The sample remaining in the boiling flask, or residue, was then distilled again at reduced pressure to measure the boiling temperatures of heavy distillate fractions. Both approaches give equivalent results once the fluid volume in the cold trap is accounted for.

The average atmospheric pressure of the high altitude laboratory at Boulder, CO (1655 m above sea level) is 83.1 kPa. The Maxwell-Bonnett correlation was applied to the ambient and reduced pressure data to convert the values to their equivalents at sea level.⁶⁵ This correlation is widely used in the petroleum industry to convert distillation curves measured at one pressure to another.^{65,66} The sea level atmospheric pressure boiling curve data can then be used with the Riazi sulfur content model.

2.2. Measurement of Residue Mass, Density, and Volume.

The principle of mass conservation dictates that the sum of the masses in the distillate (receiver), residue (boiling flask), and condensate (cold trap) fractions must be constant. Similarly, assuming that no

thermal cracking has taken place and that changes in excess volume are negligible, the measured sum of liquid volumes should also be constant. By measuring the mass and volume of the distillate and residue fractions, it is possible to calculate changes in the density of the two fractions at the end of each distillation. Changes in the postatmospheric distillation residue mass were measured by weighing the flask on a triple-beam balance. To avoid errors introduced by incomplete mass transfer from one container to another, the residue was not removed from the boiling flask for measurement. Instead, the mass of the boiling flask was subtracted from the total weighed mass to determine the change in residue mass.

The density of the postvacuum distillation residue was measured directly through pycnometry. The postvacuum distillation residue, which is highly viscous and opaque, was heated to 100 °C to reduce its viscosity. The heated residue was then drawn up into a Pasteur pipet under vacuum, with a pressure differential up to 83 kPa (0.82 atm), to the point of positive constriction near the top of the glass pipet. The residue density was calculated from the change in pipet mass when it is filled with residue, with reference to its mass when it was filled with deionized water to the same fiducial constriction. The measured mass and density of the residue can then be used to calculate its volume.

2.3. Gas Chromatography with Mass Spectrometric Detection (GC-MS). Small aliquots (10 μL) of the light distillate fractions were withdrawn at predetermined distillate volume fractions with a standard chromatography syringe in the receiver adapter hammock and dissolved in a fixed quantity of *n*-tetradecane inside an autosampler vial. The diluted aliquots were analyzed using GC-MS (30 m column with a 250 μm film of 5% phenyl-95% dimethylpolysiloxane, helium carrier gas at 34.5 kPa or 5 psi inlet pressure, split ratio of 100:1, temperature program starting at 40 °C for 4 min followed by a fast ramp-up to 190 °C at a heating rate of 20 °C/min).⁶⁷ Mass spectrometric detection was used to characterize the components of the aliquot.

Linear *n*-alkane peaks in the sample were identified using mass spectrometry. Their retention times were used to calculate the programmed-temperature retention indices (I^T) of other peaks present in the gas chromatogram. The calculated programmed-temperature retention indices were used to narrow down candidate compounds in conjunction with mass fragmentation pattern matching with the NIST 11 Mass Spectral Library to identify the compounds present in the aliquot.⁶⁸

2.4. Gas Chromatography with Flame-Ionization Detection (GC-FID). Aliquots of heavy distillate cuts were collected with a pressure-balanced syringe at the receiver adapter hammock,^{57,58} injected into an autosampler vial, and weighed on an analytical balance. The aliquot was then diluted with a fixed quantity of *n*-hexane (~1 mL), crimp-sealed, and weighed again. The diluted aliquots were analyzed through gas chromatography with flame-ionization detection (30 m column with a 250 μm film: stabilized equivalent of 5% phenyl-95% dimethylpolysiloxane, nitrogen carrier gas at 207 kPa or 30.0 psi inlet pressure, temperature program from 50 to 400 °C at a heating rate of 5 °C/min).⁶⁷ Aliquots were withdrawn at predetermined distillate volume fractions for composition analysis. The programmed-temperature retention indices of peaks present in the chromatogram were determined by injecting a calibration standard prepared from commercially procured *n*-alkanes. Column-induced artifacts (baseline drift and polysiloxane peaks), observed in blank runs with no sample injection, were removed digitally prior to data analysis.

2.5. Sulfur Chemiluminescence Detection. Distillate aliquots were collected with a chromatography syringe or pressure-balanced syringe at the receiver adapter hammock. The aliquots were then added to autosampler vials containing a fixed volume of *n*-hexane. Vials were weighed on an analytical balance prior to and after adding the sample and solvent. The mass of the sample and solvent were used to calculate the sample sulfur content based on the measured sulfur concentration in solution. Due to the propensity of sulfur compounds to adsorb on glass and metal surfaces, the aliquots were analyzed immediately after sampling. The postdistillation residue in the boiling flask was sampled with a Pasteur pipet and dissolved in *n*-hexane for analysis. The total sulfur content of each diluted aliquot was analyzed

with a gas chromatograph equipped with a sulfur chemiluminescence detector (SCD). The inlet was connected to the detector with a short retention gap instead of a chromatography column (fused silica capillary, 1 m \times 0.25 mm, nitrogen carrier gas at 41.4 kPa or 6.0 psi inlet pressure, split ratio of 0.5:1, column temperature at 200 °C, and detector temperature at 250 °C). Background correction was performed with *n*-hexane; the small, nonzero response of the sulfur chemiluminescence detector to *n*-hexane was subtracted from each of the sample values to obtain the corrected sulfur signal. The total sulfur concentration in each vial was calculated by use of a standard curve prepared with solutions of thiophene dissolved in *n*-hexane,⁶⁹ which was calibrated with a low-level sulfur in kerosene standard reference fluid (NIST SRM 1616b).

2.6. Copper Corrosion Test. A second set of 10 μL aliquots for corrosion testing was collected concurrently with the aliquots collected for SCD analysis, in the same manner as described in section 2.5. The aliquots were injected into vials containing prepared copper disks and a fixed quantity (~1 mL) of iso-octane. The copper disks were punched from sheet electrolytic tough pitch copper, polished with 65- μm grade (220 grit) silicon carbide paper, and roughened with 105- μm silicon carbide grains (from 120 grit paper) on absorbent cotton applicators wetted with iso-octane as described in ASTM D1838-12.⁷⁰ 20 μL of deionized water were injected into each iso-octane solution to promote the formation of sulfur compounds that are corrosive to copper. The vials were then crimp-sealed and placed in a water bath at 37.9 °C (100 °F) for one hour. The expanded uncertainty of the temperature was found to be 0.5 °C (1 °F), which was within the limit specified by the test method. At the end of the prescribed time, each copper disk was removed and dried in air.

The copper disks were imaged with a charge-coupled device (CCD) digital camera using the same geometry and lighting conditions described in an earlier paper (see the Supporting Information for additional details).⁵⁰ The images were processed to transform digital image data collected in the red-green-blue (RGB) color space to the $L^*a^*b^*$ color space.^{71,72} The $L^*a^*b^*$ color space uses lightness (L^*), red-green (a^*), and yellow-blue (b^*) color-opponent axes to encode colors in a perceptually linear manner that most closely approximates human visual perception. The ASTM Copper Strip Corrosion Standard lithograph was imaged under the same conditions as the copper disks. The $L^*a^*b^*$ values were used to develop a vector representation of reference strip classifications in color space. Copper disks were assigned categorical corrosion ratings by comparison with the ASTM Copper Strip Corrosion Standard. Assignments were made by calculating the distance between the $L^*a^*b^*$ vector of each copper disk and all reference vectors and finding the reference vector that is the closest match to the copper disk vector values in $L^*a^*b^*$ color space.

3. RESULTS AND DISCUSSION

3.1. Characterization of Crude Oil Properties. The bulk density of the composite petroleum sample was measured through pycnometry. The vial volume was calibrated by measuring the increase in mass when the vial was filled with deionized water at ambient conditions (22.6 °C and 83.18 kPa). Once the volume of the vial was determined, the vial was dried, refilled with petroleum, and weighed again. The density of the petroleum was found to be 0.8735 g/cm³ with a combined uncertainty of 0.0001 g/cm³ at 22.6 °C, which is equivalent to a specific gravity of 0.8783 at 20 °C or an API gravity of 29.94° at the same temperature. Because the density is derived from the measured volume of the container and the mass of the sample, the uncertainty estimate of the two measured values is combined in quadrature to determine the uncertainty of the density. All of the uncertainties reported in this work are estimates of an expanded uncertainty (U) with a coverage factor of 2 (i.e., $2 u_c$, where u_c is the combined

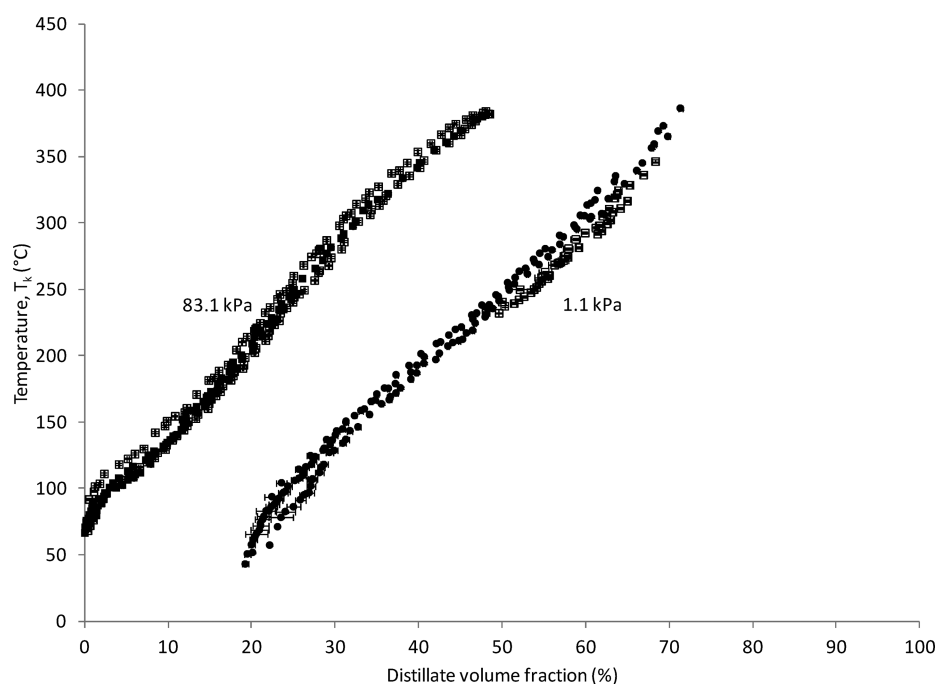


Figure 2. Distillation curve data for a composite North American crude oil sample at 83.1 kPa (with an expanded uncertainty of 0.7 kPa) from 0 to 45% distillate volume fraction and 1.1 kPa (with an expanded uncertainty of 0.7 kPa) from 19 to 70% distillate volume fraction. Here, the temperature of the liquid in the boiling flask (kettle) is plotted as a function of distillate volume fraction. Open symbols represent atmospheric pressure distillations followed by reduced pressure distillations. The expanded uncertainties in the measurement are typically smaller than the plotting symbols in the figure.

standard uncertainty), corresponding to a level of confidence of approximately 95%.⁷³

The mineral content of the petroleum was measured through wet-ashing and X-ray analysis. The sample was first charred with concentrated sulfuric acid and heated to 540 °C for 6 to 12 h in a quartz beaker.⁷⁴ The mean ash content of three replicate measurements was 0.0210% (mass/mass), with a combined expanded uncertainty of 0.028% (mass/mass). X-ray energy dispersive spectroscopy of the ash showed trace quantities of vanadium, silicon, nickel, iron, and calcium to be present in the sample.

3.2. Boiling Temperature As a Function of Distillate Volume. The atmospheric and reduced pressure distillation data are shown graphically in Figure 2. For the ADC method, we typically record the temperatures at which we visually observe (a) the onset of bubbling, (b) sustained bubbling, and (c) the temperature at which vapor is observed to rise into the distillation head. The onset of bubbling and sustained bubbling temperatures are useful as diagnostics during distillation. The vapor rise temperature is the theoretically significant initial boiling temperature (IBT) of the complex fluid. This temperature is important because the sample composition in the boiling flask is fixed and measurable at the start of the distillation; therefore, the data can be used to develop an equation of state. The measured IBT values are provided in Table 1. It should be noted that the T_h thermocouple as well as the distillation head were initially at ambient temperature (approximately 20 °C) at the start of the distillation. For distillations started at -100 °C, the vapor from the low boiling-point compounds actually cools the T_h thermocouple and causes its temperature to dip. This behavior is contrary to the usual increase in temperature observed for fluids with boiling temperatures higher than the ambient temperature.

Table 1. Vapor Rise or Initial Boiling Temperature (IBT) for a Composite North American Crude Oil Sample Based on the Average of Three Replicates for Reduced Pressure Distillation and Four Replicates for Atmospheric Pressure Distillation^a

pressure (kPa)	$U(P)$ (kPa)	IBT (°C)	$U(T)$ (°C)
1.1	0.7	-32.0	28.0
83.1	0.7	66.3	7.0

^aThe expanded uncertainty (U) shows the combined standard uncertainty with a coverage factor of 2, corresponding to a level of confidence of approximately 95%.

The difference in boiling temperature between the atmospheric pressure distillation curve and reduced pressure distillation curve is approximately 150 °C in the 20% to 50% (volume/volume) range. In general, decreasing the pressure shifts the temperatures of the distillation curve to lower values without changing the curve shape. This behavior was observed in the composite North American petroleum sample and is consistent with the general principle.

The Maxwell-Bonnell correlation was used to convert all distillation curve data to atmospheric pressure at sea level. The converted data, shown in Figure 3, show a strong positive linear correlation between the boiling temperature and the distillate volume fraction. The data can be described by a linear function of distillate volume fraction with a slope of 6.500 °C per unit distillate volume fraction in % (volume/volume) and an intercept of 84.311 °C, where the uncertainties in the coefficients are 0.034 and 1.234 °C, respectively, at the 95% confidence level.

3.3. Composition and Average Molecular Mass of Distillate Fractions. The composition-explicit data channel in the ADC method is a powerful tool in the analysis of complex

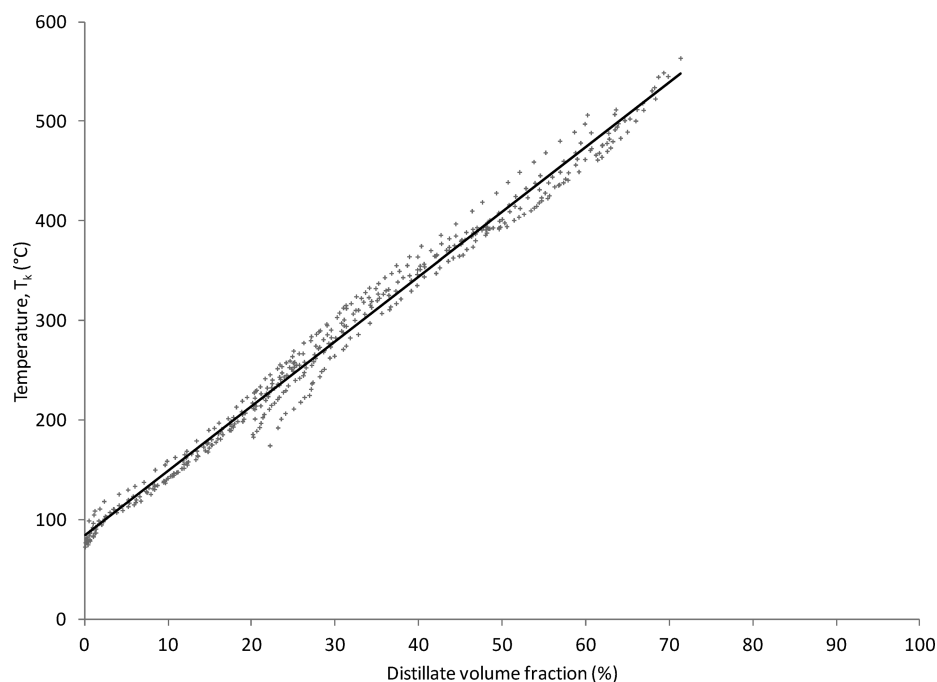


Figure 3. Distillation curve data for a composite North American crude oil sample converted to sea level atmospheric pressure with the Maxwell-Bonnett correlations. The data comprises seven distillation measurements at ambient and reduced pressures. A strong positive linear correlation exists between the boiling temperature and the distillate volume fraction. See text for discussion of uncertainty in the linear regression coefficients.

fluids when coupled with other observations. The aliquots drawn during distillation can be analyzed using a variety of approaches to determine their composition and properties, including GC-MS and GC-FID. Programmed-temperature GC was used to separate the components of each distillate fraction taken during ADC measurement. In the early fractions (Figure 4), individual compounds can be identified through their mass fragmentation patterns and programmed-temperature retention indices (see the Supporting Information, section S2, for additional details). Analysis of these light fractions, ranging from 5.8% to 24.5% distillate volume fraction, shows a strong positive linear correlation between I^T and average molecular mass of a distillate fraction, summarized in Table 2 and plotted in Figure 5. This result is consistent with the positive linear correlations known to exist between the chromatographic retention index of a compound, its molecular mass, and its boiling temperature.

Misidentification of the individual components in a chromatogram and overlapping peaks are the largest sources of error in estimating the average molecular mass of a fraction based on its composition. The number of hydrocarbon isomers grows rapidly with the number of carbons and functional groups present. Fortunately, structural isomers all have the same molecular mass. Misidentification of one structural isomer for another has minimal effect on the outcome of the analysis for this reason. In addition, the mass fragmentation patterns of linear *n*-alkanes and branched iso-alkanes are readily distinguished from each other, as are those of molecules containing cyclic, aromatic, and thiol functional groups. The distinct mass fragmentation patterns reduce the likelihood of misidentifying the category or class of a petroleum component; however, the mass of molecules within a class of compounds differing by one carbon can be difficult to discern through fragmentation patterns alone. This is particularly true when the molecular ion peak is absent or low in intensity.

The difficulty of distinguishing molecules that differ by one carbon within a class of compounds was addressed by referencing its programmed-temperature retention index.^{68,75} The isothermal Kovats retention index and the related programmed-temperature retention index of a compound depend on the strength of its interaction with the stationary phase in a GC column.⁷⁶ Group contribution or quantitative structure property relationship (QSPR) approaches to boiling temperature and retention time estimation have been found to be a useful analytical tool in identifying individual components of a mixture herein.^{77,78}

The average molecular mass of a distillate fraction is obtained by summing the molecular mass of each identified component, weighted by its peak area as a fraction of the sum of all peaks present in the chromatogram. The error due to peak misidentification is estimated by calculating the standard deviation of three molecular masses: the molecular mass of the identified compound and the molecular masses of the two closest peaks. This line of thought likely overstates the error from peak misidentification, as structural isomers are more likely to coelute and have no effect on the molecular mass.

Heavy fractions, which contain numerous coeluting compounds in the form of a broad unresolved complex mixture (UCM) hump (Figure 6), defy analysis through this approach. Instead, the mean retention time of the Gaussian or bell-shaped curve relative to the *n*-hexane solvent peak was measured by fitting a normal distribution curve to the detector output data. These retention times were converted to programmed-temperature retention indices with reference to the retention times of *n*-alkanes in a calibration standard. The linear relationship between the mean I^T and molecular mass developed previously from light fraction data was then used to estimate the average molecular mass of the heavy fractions based on the UCM mean retention times. The values are

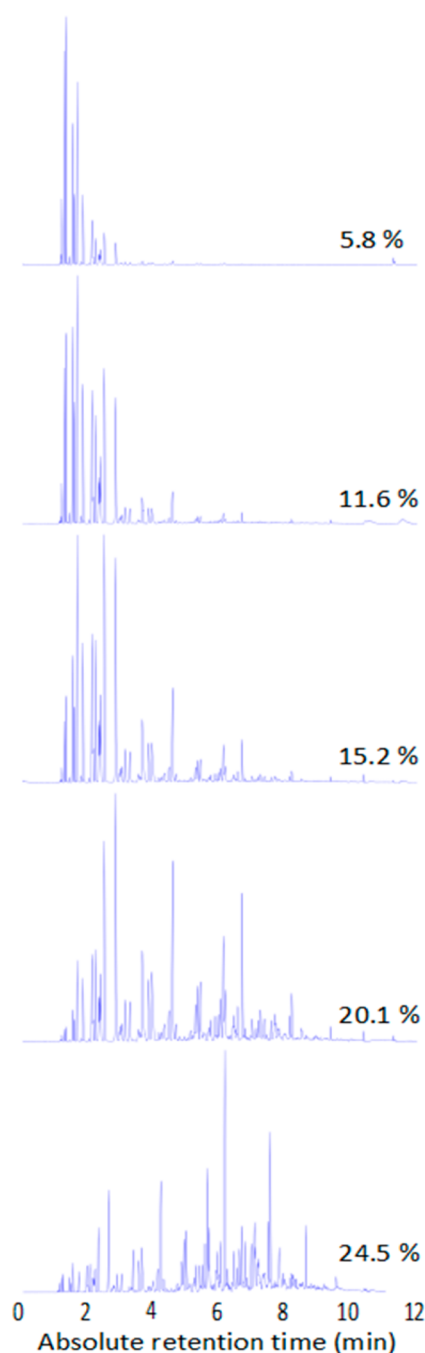


Figure 4. Chromatograms of light distillate fractions of a composite North American crude oil sample, plotted as total-ion count as a function of absolute retention time. Percentages reflect distillate volume fraction. The *n*-tetradecane solvent signal has been subtracted to remove the background and trace contaminant peaks.

reported in Table 3 and plotted along with the light fraction data as a function of distillate volume fraction in Figure 7.

The mean molecular mass of distillate aliquots determined through GC-MS and estimated from GC-FID data appear to be mutually consistent, and both data sets can be described by the same second-order polynomial function. The function, $f(x) = ax^2 + bx + c$, was fitted to the combined data set in the range of 0.2% to 72% distillate volume fraction, and the coefficients were found to be $a = 0.0881$, $b = -0.641$, and $c = 79.06$. The

Table 2. Distillate Volume Fraction, Weighted-Average Programmed-Temperature Retention Indices (I^T), and Molecular Mass (M) of Light Fractions Analyzed with GC-MS^a

distillate volume (%)	$U(V)$ (%)	I^T	$U(I^T)$	M (g/mol)	$U(M)$ (g/mol)
0.17	0.10	434	6	65.2	6.4
0.22	0.10	447	7	66.3	6.7
0.31	0.10	455	6	67.8	6.2
1.21	0.40	488	7	72.6	7.5
5.79	0.40	568	6	82.3	4.9
11.62	0.10	655	5	93.2	3.5
15.16	0.09	721	5	102	3
20.08	0.07	801	5	113	3
24.50	0.06	866	5	124	3
26.89	0.56	1055	14	143	6
32.74	0.29	1145	9	153	6

^aThe expanded uncertainty (U) shows the combined standard uncertainty with a coverage factor of 2, corresponding to a level of confidence of approximately 95%.

uncertainties in the coefficients are 0.0128 (14.5%), 0.901 (140%), and 13.4 (16.9%), respectively.

3.4. Distillate Fraction and Residue Fraction Densities As a Function of Distillate Volume. Approximately 30% (volume/volume) of the petroleum sample remained in the boiling flask at the end of each reduced pressure distillation, as determined through pycnometry and residue mass. Up to 24 mL of condensate was recovered from the cold trap when the distillation was started at -100 °C under reduced pressure. The condensate volume was significantly lower when compared with atmospheric pressure distillations, which typically result in less than 0.3 mL recovered from the cold trap.

The density of the petroleum sample remaining in the boiling flask at the end of each distillation, or the postdistillation residue, was measured through pycnometry. A strong positive linear correlation exists between the residue density and distillate volume fraction. This result can be explained by the fact that smaller and lighter hydrocarbon molecules tend to have lower boiling temperatures than larger and heavier molecules and are preferentially transferred to the distillate fraction during distillation. The residue fraction density is always greater than the distillate fraction density for this reason.

The composition of light distillate fractions identified through GC-MS can be used to estimate other properties based on published thermophysical data of individual components. The Thermodynamics Research Center (TRC) at NIST provides critically evaluated thermodynamic data on organic compounds in a searchable online database.^{79,80} Estimated densities of light distillate fractions based on weighted-averages from GC-MS composition data and critically evaluated thermophysical data are reported in Table 4, as are measured densities of residue fractions. When calculating the changes in density of the distillate fraction, the contribution due to changes in the mixture excess volume is expected to be small.

Changes in the volumes and densities of the distillate fractions and residue fractions during distillation are constrained by the conservation of mass. Mass gained by the distillate fraction must be balanced by a loss of mass from the residue fraction. Since the reduced pressure ADC apparatus approximates a closed system for mass transfer, it is possible to

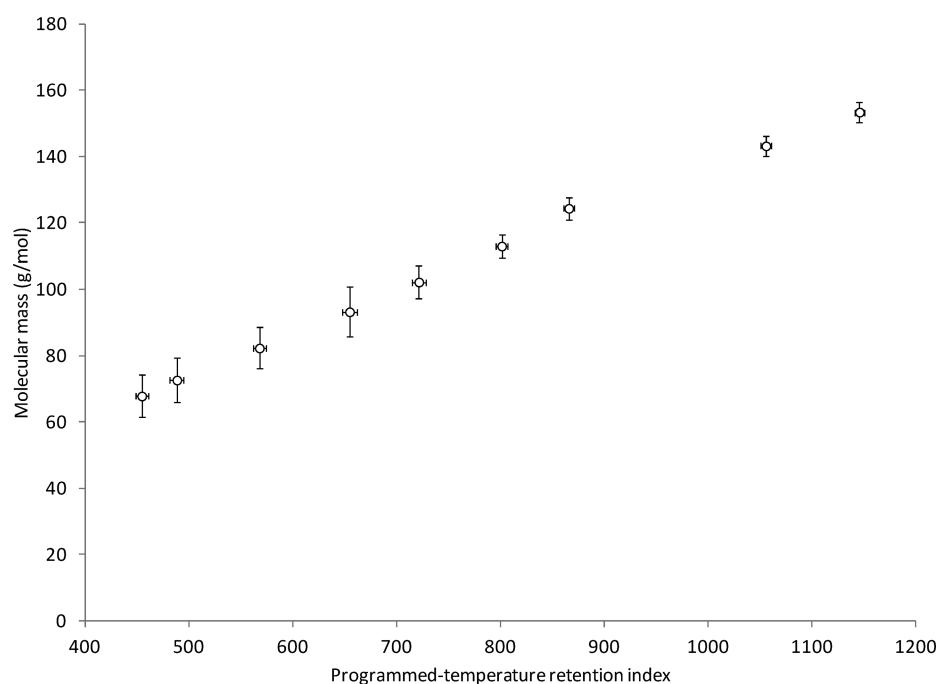


Figure 5. Average molecular mass of distillate fractions from 0.2% to 42% (volume/volume) of a composite North American crude oil sample based on analysis of GC-MS data plotted as a function of their programmed-temperature retention index (I^T).

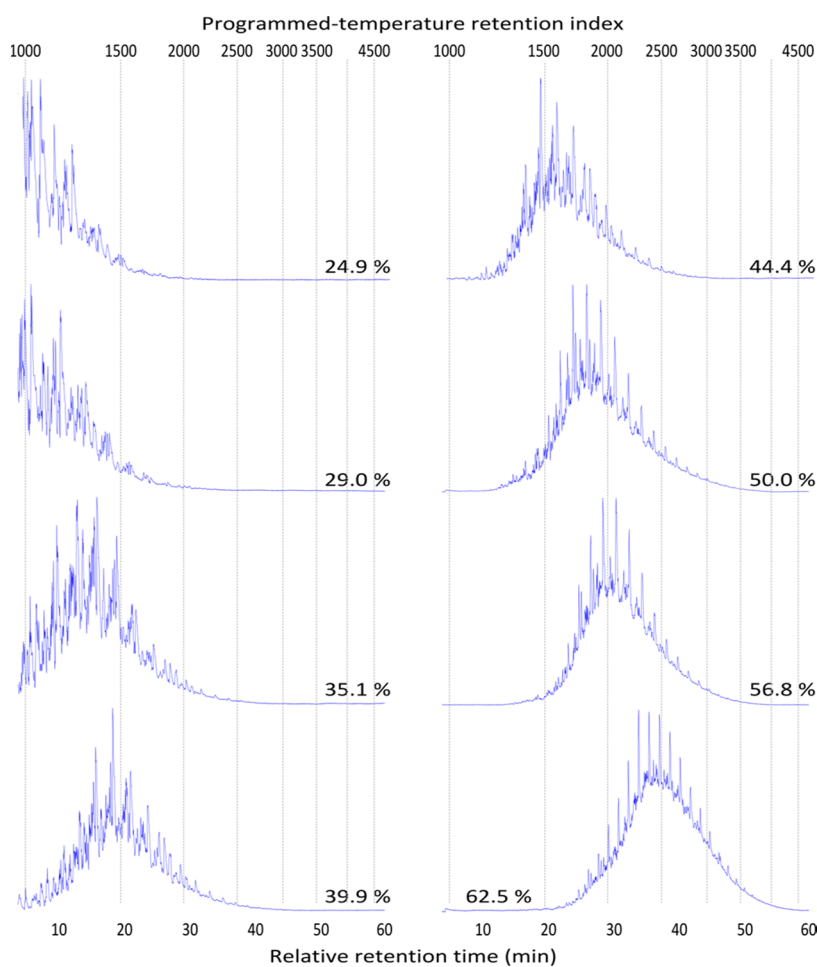


Figure 6. Chromatograms of heavy distillate fractions of a composite North American crude oil sample, plotted in arbitrary units of intensity (based on flame-ionization detector current output) as a function of absolute retention time. Column bleed, contributing to an increase in the background signal, has been removed through digital data processing. Vertical lines represent retention times of n -alkane I^T standards.

Table 3. Distillate Volume Fraction, Weighted-Average Programmed-Temperature Retention Indices (I^T) and Molecular Masses (M) of Heavy Fractions Analyzed with GC-FID Based on Two Replicates^a

distillate volume (%)	$U(V)$ (%)	I^T	$U(I^T)$	M (g/mol)	$U(M)$ (g/mol)
35.1	0.1	1409	34	188	10
39.8	0.1	1562	33	207	10
44.3	0.2	1682	33	223	10
50.2	0.4	1918	32	252	10
55.4	0.7	2135	31	279	11
60.8	0.4	2550	29	332	11
65.0	0.4	2925	28	379	12
69.6	0.1	4163	25	534	13

^aThe expanded uncertainty (U) shows the combined standard uncertainty with a coverage factor of 2, corresponding to a level of confidence of approximately 95%.

calculate the distillate mass by the difference in the sample mass in the boiling flask at the start and end of the distillation. The densities of the two fractions can be calculated if volume changes are negligible for both fractions. The volume may be affected by hydrocarbon cracking or changes in the mixture excess volume. The volume change due to hydrocarbon cracking should be negligible, as a limit was placed on the distillation temperature; the change in the mixture excess volume is expected to be minimal, as explained below.

For binary mixtures of n -alkanes, the maximum mixture excess volume is approximately $-0.14 \text{ cm}^3/\text{mol}$;⁸¹ for mixtures of cyclohexane and alkanes, the mixture excess volume ranges from -0.3 to $0.7 \text{ cm}^3/\text{mol}$.⁸² The change in the mixture excess volume during distillation of a distillate cut is estimated to be

less than $0.004 \text{ cm}^3/\text{mol}$. In a complex fluid, each component constitutes only a small fraction of the total volume. Compositional changes to the concentration of one component during distillation must be smaller than the concentration of the component in the complex fluid. The estimated changes in the mixture excess volume are comparable in magnitude to the expanded uncertainty of the volume measurements in the ADC receiver. Changes in the total sample volume from the start to the end of the distillation were found to be statistically insignificant for measurements made in the reduced pressure ADC apparatus.

Figure 8 summarizes the changes in residue fraction and distillate fraction densities as a function of distillate volume fraction. The light distillate fraction densities, estimated from GC-MS and thermophysical data, were used to calculate the residue fraction densities for corresponding distillate volume fractions. The calculated values for the residue fraction are in agreement with values measured through pycnometry. The distillate fraction density increases asymptotically as a function of distillate volume fraction and can be described by a function of the form $f(x) = a - b/(x + c)$, where the coefficients are $a = 0.84153$, $b = 3.21068$, and $c = 13.30303$. The function is constrained not only by the distillate fraction density data but also the residue fraction density data. The residue fraction density is not a free parameter but a function of mass transfer during distillation. The density of the residue fraction was evaluated by numerically integrating the distillate fraction density function to obtain the change in sample mass and then dividing the decreased sample mass by the residue volume calculated by subtracting the distillate volume from the initial volume.

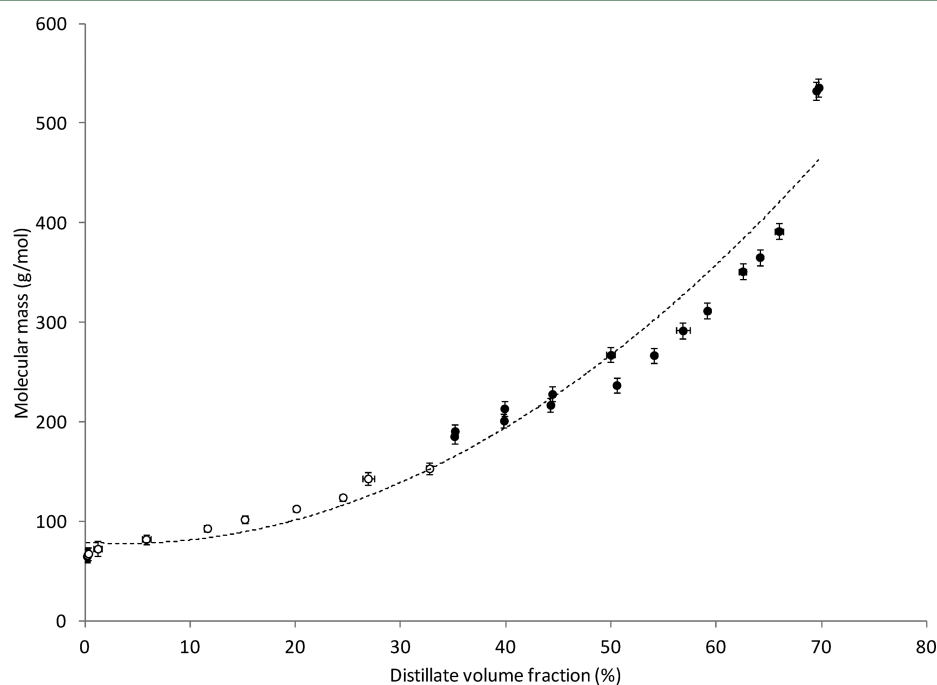


Figure 7. Average molecular mass of distillate fractions of a composite North American crude oil sample based on analysis of GC-MS and GC-FID data plotted as a function of distillate volume fraction. Open circles (O) indicate estimates derived from a weighted-average sum of contributions from compounds identified through GC-MS; closed circles (●) show average molecular mass estimates derived from the linear relationship developed from Figure 4 and mean unresolved complex mixture (UCM) retention time from Figure 5. The dashed line represents a linear second-order regression line based on a least-squares fit of both data sets. Bars showing expanded uncertainty are smaller than plotting symbols when they are not visible. See text for additional discussion of uncertainty.

Table 4. Distillate Fraction Density (ρ_d) and Residue Fraction Density (ρ_r) of a Composite North American Crude Oil Sample at Different Distillate Volume Fractions^a

distillate volume (%)	$U(V)$ (%)	ρ_d (g/cm ³)	$U(\rho_d)$ (g/cm ³)	ρ_r (g/cm ³)	$U(\rho_r)$ (g/cm ³)
Estimated from GC-MS Composition Data and Critically Evaluated Density Values					
0.3	0.1	0.6048	0.0006	0.8784	0.0006
5.8	0.1	0.6688	0.0005	0.8870	0.0005
11.6	0.2	0.7108	0.0003	0.8934	0.0003
15.2	0.4	0.7352	0.0004	0.8990	0.0004
20.1	0.7	0.7557	0.0006	0.9050	0.0006
24.5	0.4	0.7722	0.0009	0.9105	0.0009
Pycnometry Measurement					
0 (bulk)				0.87349	0.00004
25.4	0.1			0.906	0.004
49.6	0.1			0.973	0.004
50.4	0.1			0.973	0.004
51.2	0.1			0.984	0.004
68.3	0.1			1.010	0.004
69.5	0.1			1.008	0.006
69.7	0.1			1.030	0.006
74.7	0.1			1.024	0.004
75.1	0.1			1.033	0.004

^aDistillate fraction density values are estimated from the weighted-average densities based on peak composition and critically evaluated density values (see text for Discussion). The mass conservation principle was applied to derive the corresponding residue density values for the given distillate volume fractions. Density values measured through pycnometry are reported in the second part of the table. The expanded uncertainty (U) shows the combined standard uncertainty with a coverage factor of 2, corresponding to a level of confidence of approximately 95%.

Interestingly, the measured residue density values in the 50% to 75% volume fraction range suggest an asymptotic limit to the distillate fraction density around 0.841 g/cm³. This constraint makes sense given that the distillate fraction density must approach the initial bulk density, 0.873 g/cm³, in the ideal case where the entire mass of the petroleum sample in the boiling flask is transferred to the distillate fraction in the receiver at the end of distillation. Divergence from this ideal case is marked by a pronounced upturn in the residue density in this model beyond 75% distillate volume fraction, assuming that the distillate fraction density continues to approach 0.841 g/cm³ asymptotically. The residue density approaches the density of petroleum coke⁸³ and solid graphite,⁸⁴ the limiting case, as distillate volume fraction approaches unity.

3.5. Estimated Refractive Indices of Light Distillate Fractions. The refractive index of a distillate fraction depends strongly on its composition.⁶⁵ Using the composition data obtained through GC-MS, the refractive indices of the light distillate fractions were estimated using the same weighted-average approach used to estimate their densities. Estimated refractive indices based on GC-MS data and critically evaluated thermophysical data are reported in Table 5. The estimated values are in agreement with the values predicted by the Riazi-Daubert correlation between refractive index, boiling temperature, and density, as shown in Figure 9.⁸⁵ Table 6 summarizes the boiling temperature, density, and refractive index values as a function of distillate volume fraction. As discussed in section 3.1, the boiling temperature is a linear function of distillate volume fraction

$$T_b = 6.500V + 84.311 \quad (1)$$

where T_b is the boiling temperature in °C, and V is the distillate volume fraction in % (volume/volume). Derivation of the

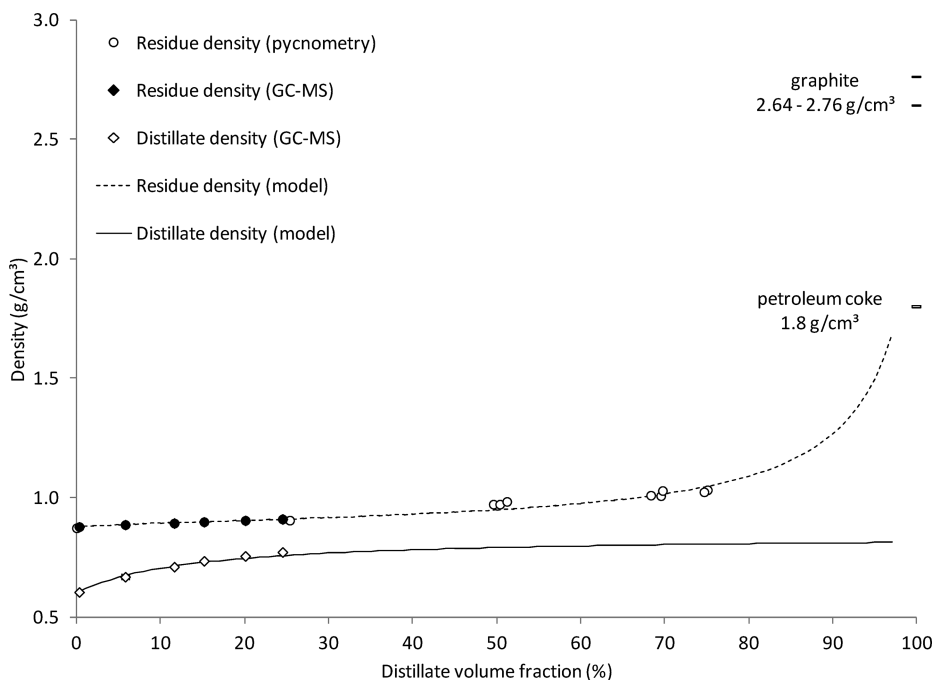


Figure 8. Distillate fraction density and residue fraction density of a composite North American crude oil sample plotted as a function of distillate volume fraction. See text for additional discussion on the density modeling and constraints placed on distillate fraction density for distillate volume fractions in the range of 50% to 75% (volume/volume). The densities of petroleum coke⁸³ and graphite⁸⁴ are plotted for reference at the end of the distillation range.

Table 5. Refractive Index (nD20) at 589 nm and 20 °C of Light Fractions Based GC-MS Composition Data and Critically Evaluated Refractive Index Values^a

distillate volume (%)	U(V) (%)	nD20	U(nD20)
0.31	0.1	1.3439	0.0007
5.79	0.1	1.3784	0.0001
11.62	0.2	1.3975	0.0001
15.16	0.4	1.4103	0.0001
20.08	0.7	1.4220	0.0001
24.50	0.4	1.4324	0.0002

^aThe expanded uncertainty (U) shows the combined standard uncertainty with a coverage factor of 2, corresponding to a level of confidence of approximately 95%.

distillate density function is described in section 3.3. The function has the following form

$$\rho = 0.84153 - 3.21068/(V + 13.30303) \quad (2)$$

where ρ is the density in g/cm^3 at 20 °C, and V is the distillate volume fraction in % (volume/volume). Density values can be converted to specific gravity at 15.5 °C using the following approximation, which accounts for the decrease in density with increase in temperature in hydrocarbons:⁶⁵

$$\text{SG} = 0.9915\rho + 0.01044 \quad (3)$$

Refractive index values calculated from the boiling temperature and density, based on the Riazi-Daubert empirical correlation, are reported in Table 6 due to the lack of composition data beyond the 25% distillate volume fraction in this study.

3.6. Estimated and Measured Sulfur Content. The distillate volume fractions in Table 6 correspond to sampling points for sulfur content and corrosivity measurements described in sections 2.5 and 2.6. Predicted and measured sulfur mass concentration, expressed as % (mass/mass), are

plotted as a function of distillate fraction in Figure 10. The SCD data agree closely with the values predicted by the Riazi-Daubert correlation up to 60% distillate volume fraction. The total sulfur concentration of the petroleum sample is estimated to be 1.36% (mass/mass), with an absolute average deviation of 0.15% (mass/mass) and expanded uncertainty less than 0.30% (mass/mass). The predicted value is consistent with the measured value of 1.13% (mass/mass), with an expanded uncertainty of 0.21% (mass/mass).

The increase in the sulfur content with distillate volume fraction can be explained by the presence of large asphaltene molecules in the residual oil fraction. Asphaltenes contain from 0.3 to 10.3% (mass/mass) sulfur. The sulfur is incorporated into the polycyclic aromatic hydrocarbon structure of asphaltenes as heteroatoms, which are difficult to remove through heating alone.⁸⁶ Sulfur present in the petroleum becomes concentrated in the vacuum residue fraction, consistent with prior observations in our lab of high sulfur content in heavy fuel oil for marine diesel engines.⁴²

3.7. Copper Coupon Corrosion. The $L^*a^*b^*$ values of the ASTM copper corrosion standard strips are presented in Table 7 and plotted in Figure 11 with reference to the values of a pristine copper strip. The classification of copper strips in ASTM D1838 proceeds from slight tarnish (1), moderate tarnish (2) to dark tarnish (3), followed by corrosion (4). The $L^*a^*b^*$ vectors of reference strip appear to trace a downward counterclockwise spiral about the lightness axis centered on the values for the pristine copper strip. The uncertainty values reported in Table 7 demarcate “bins” in vector space for the classification of the copper strips. Corrosion of copper disks in contact with diluted distillate, in a modified ASTM D1838–12 copper strip corrosion test, showed only slight tarnish (1a) for the majority of samples tested, as seen in Table 8. The only exception occurred for the sample at 50.5% (volume/volume) distillate volume fraction, which produced more tarnish (1b) when compared with other samples.

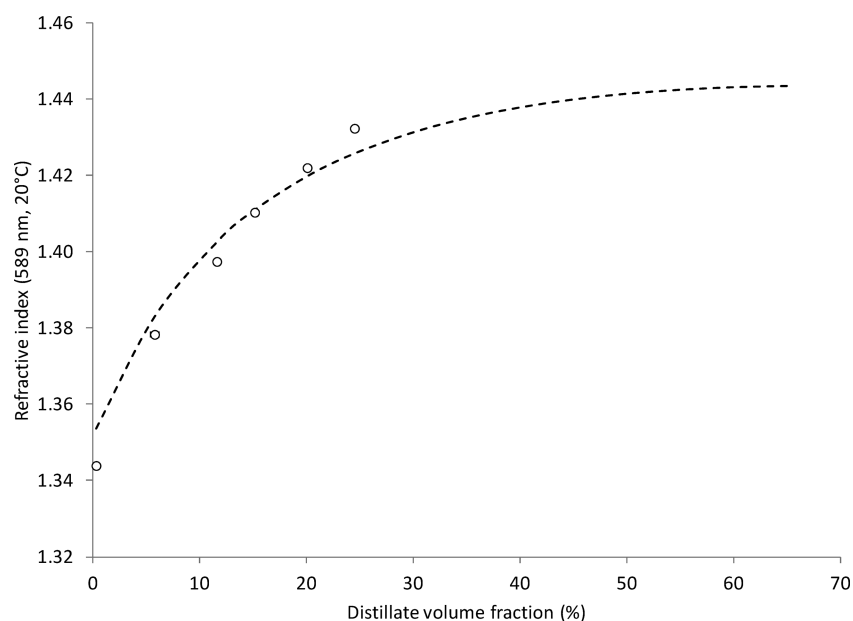


Figure 9. Refractive index (nD20), at 589 nm and 20 °C, of a composite North American crude oil sample plotted as a function of distillate volume fraction based on GC-MS composition data and critically evaluated refractive index values. The dashed line shows predicted refractive values based on an empirical model that uses boiling point and density as input parameters.⁸⁵ The expanded uncertainties in the measurement are smaller than the plotting symbols in the figure.

Table 6. Sulfur Content Expressed As Percent by Mass of a Composite North American Crude Oil Sample, As Estimated (S_{est}) from Boiling Point (T_k), Density (ρ), and Refractive Index (nD20) Functions and Measured Directly Using Sulfur Chemiluminescence Detection (SCD)^a

V (%)	$U(V)$ (%)	T_k (°C)	$U(T_k)$ (°C)	ρ (g/cm ³)	$U(\rho)$ (g/cm ³)	nD20	S_{est} (%)	SCD (%)	$U(\text{SCD})$ (%)
0 (bulk)		66.3	7.0	0.87349	0.00004		1.36	1.13	0.21
0.05	0.4	85	2	0.60	0.018	1.352	0.00	0.01	0.72
6.7	0.1	128	2	0.68	0.008	1.387	0.00	0.00	0.68
10.7	0.1	154	2	0.71	0.008	1.400	0.00	0.00	0.66
15.2	0.1	183	2	0.73	0.008	1.411	0.00	0.00	0.71
20.2	0.1	215	1	0.75	0.008	1.420	0.00	0.01	0.72
24.8	0.1	245	1	0.76	0.008	1.426	0.00	0.01	0.75
29.0	0.1	273	1	0.77	0.008	1.430	0.00	0.04	0.80
35.1	0.1	312	1	0.78	0.008	1.435	0.00	0.10	0.84
39.8	0.1	343	1	0.78	0.008	1.438	0.03	0.16	0.85
44.2	0.1	372	2	0.79	0.008	1.440	0.13	0.23	0.87
50.5	0.2	413	2	0.79	0.008	1.442	0.24	0.41	0.88
55.0	0.4	442	2	0.79	0.008	1.442	0.31	0.51	0.89
60.1	0.4	475	2	0.80	0.008	1.443	0.38	0.85	0.90
65.1	0.4	507	3	0.80	0.008	1.443	0.43	1.71	0.92
69.7 (residue)	0.1	537	3	1.016	0.0026	1.547	3.93	2.86	0.92

^aThe total sulfur content, reported for the bulk value, is based on trapezoidal rule integration of the pseudocomponent sulfur content over the range of distillate volume fractions (V). The absolute average deviation for the Riazi sulfur content correlation is reported to be 0.15% (mass/mass), with a maximum average deviation of 1.6% (mass/mass). The expanded uncertainty (U) shows the combined standard uncertainty with a coverage factor of 2, corresponding to a level of confidence of approximately 95%.

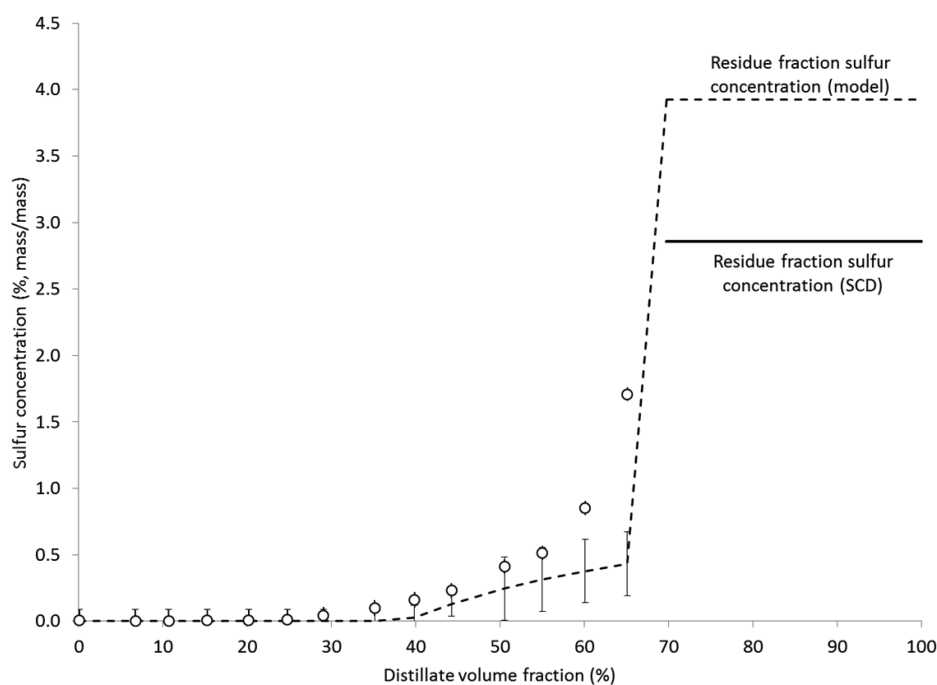


Figure 10. Sulfur content expressed as percent by mass of a composite North American crude oil sample, plotted as a function of distillate volume fraction. Open circles (O) indicate SCD data; the dashed line represents the Riazi sulfur correlation model, plotted with error bars showing absolute average deviations of 0.09% for average molecular masses from 76–247 g/mol and 0.24% for average molecular masses from 230–1500 g/mol. Residue sulfur concentrations plotted as percent by mass is shown as a solid line for volume fractions greater than 70%. Total sulfur content is obtained by numerically integrating the sulfur concentration over the entire volume range.

The discrepancy may be explained by the two-distillations approach described in section 2.1. The sample drawn at 50.5% was obtained when the boiling flask was at a temperature of 384.2 °C, with an expanded uncertainty of 0.9 °C. The temperature was near the upper limit of the distillation temperature range (400 °C). The residue from the ambient pressure distillation was allowed to cool to room temperature before the system pressure was brought down to 13 kPa and

the residue distilled under reduced pressure. The next three corrosivity samples, obtained at 54.1%, 59.1%, and 64.1% (volume/volume), all contained higher concentrations of sulfur by mass, yet produced only slight tarnish (1a) of the copper coupons. This is possibly due to the lower boiling temperatures of these fractions at reduced pressure, which were not high enough to cause cracking of sulfur–carbon bonds in high molecular mass asphaltene molecules. Alternately, it is also

Table 7. Average Lightness (L^*), Red-Green (a^*) and Yellow-Blue (b^*) Values of ASTM Copper Strip Corrosion Standard Reference Strips, Based on Five Replicate Images of the Strips Rotated through 90° ^a

designation	classification	L^*	$U(L^*)$	a^*	$U(a^*)$	b^*	$U(b^*)$
pristine		351.2	98.3	34.4	26.0	232.1	20.4
slight tarnish	1a	343.7	95.4	46.0	21.9	246.9	37.7
	1b	335.2	76.5	57.3	12.6	257.6	43.8
moderate tarnish	2a	275.9	36.6	202.2	21.7	207.7	20.8
	2b	296.3	38.0	109.4	12.4	158.7	8.8
	2c	234.5	25.7	63.7	12.3	99.6	15.7
	2d	338.6	46.4	7.1	4.1	199.6	13.6
	2e	329.8	41.8	18.2	2.6	235.4	28.4
dark tarnish	3a	309.1	34.8	78.5	9.4	215.3	19.4
	3b	253.0	24.4	38.2	9.0	92.9	18.1
corrosion	4a	210.0	29.3	17.7	5.9	70.1	15.2
	4b	182.1	30.2	7.2	7.5	63.0	22.5
	4c	182.2	55.3	8.8	8.6	75.7	39.6

^aThe expanded uncertainty (U) shows the combined standard uncertainty with a coverage factor of 2, corresponding to a level of confidence of approximately 95%.

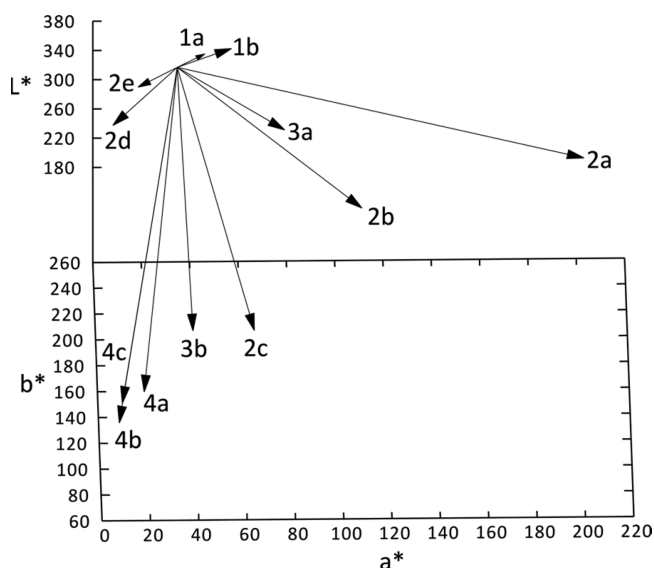


Figure 11. Vector representation of average lightness (L^*), red-green (a^*), and yellow-blue (b^*) values for the ASTM copper corrosion standard, from slight tarnish (1) to moderate tarnish (2), dark tarnish (3), and corrosion (4). The origin of the vector is the $L^*a^*b^*$ value for a pristine copper strip. Values are based on five replicates of RGB image data mathematically transformed to $L^*a^*b^*$ color space.

possible that the sulfur compounds at the higher distillate volume fractions are refractory in nature. Figure 12 summarizes the copper disk corrosion classification, sulfur content, and boiling temperature data as a function of distillate volume fraction.

4. CONCLUSIONS

In this paper, we applied the ADC method to the analysis of a composite sample of North American petroleum and measured its distillation curve at two pressures. Distillate aliquots were drawn at discrete distillate cuts and analyzed to determine their composition, sulfur content, and corrosivity. The distillation curve data showed a strong positive linear correlation between the boiling temperature and the distillate volume fraction. Since the initial boiling temperature results are thermodynamic state points, these data are amenable to the development of equation of state models for petroleum.

Composition analysis by use of GC-MS was shown to be useful in estimating the average molecular mass, density, and index of refraction for distillate cuts. Mass spectrometry was useful in determining the type of molecule present (e.g., n -alkane, isoalkane, cyclic, or aromatic), while the programmed-temperature retention index proved to be helpful in differentiating molecules differing by one carbon within a class of compounds. The programmed-temperature retention index can be calculated for all peaks in a chromatogram by using n -alkanes, which have a characteristic mass fragmentation pattern, as internal standards found within the sample.

Once identified, a weighted-average of thermophysical values can be estimated using a database of critically evaluated thermodynamic data. The estimated density based on GC-MS composition data agreed closely with residue fraction density values measured through pycnometry. A three-parameter model was developed to describe the change in the densities of distillate and residue fractions. The model suggested that the distillate fraction density asymptotically approaches a value below the initial density of the petroleum sample, while the residue fraction density approaches reported values for petroleum coke. The estimated index of refraction, based on a similar analysis of GC-MS composition data and critically evaluated thermodynamic data, agreed closely with an empirical relationship between boiling temperature, density, and refractive index published by Riazi and Daubert.⁸⁵

Gas chromatography with flame ionization detection proved to be useful in measuring the average relative retention time of the unresolved complex mixture (UCM) hump present in heavy distillate fractions. The average molecular mass of the fraction was calculated using the positive linear correlation between the average programmed-temperature retention index and average molecular mass observed in the GC-MS data set. The average molecular mass can be described as a second-order polynomial function with respect to distillate volume fraction.

Boiling temperature and molecular mass correlations were used to predict sulfur content of distillate cuts as a function of distillate volume fraction. The predicted values were in agreement with sulfur concentrations measured through sulfur chemiluminescence detection. Corrosivity, as measured by tarnishing of copper disks immersed in diluted distillate aliquots, was found to vary as a function of sulfur concentration and sampling temperature.

Table 8. Average Lightness (L^*), Red-Green (a^*), and Yellow-Blue (b^*) Values of Copper Disks Immersed in Diluted Distillate in Isooctane Drawn at Various Distillate Volume Fractions, Based on Five Replicate Images of the Disks Rotated through 90° ^a

	V (%)	U(V) (%)	L^*	U(L^*)	a^*	U(a^*)	b^*	U(b^*)	classification
A	0.05	0.4	446.6	35.6	7.1	55.2	250.5	44.0	1a
B	6.7	0.1	458.1	77.4	-13.0	132.1	237.4	105.0	1a
C	10.7	0.1	449.1	45.0	4.3	79.9	241.4	68.5	1a
D	15.2	0.1	455.3	40.0	-6.9	69.3	236.9	61.3	1a
E	20.2	0.1	459.3	46.2	-14.4	80.7	235.8	66.8	1a
F	24.8	0.1	447.9	64.7	5.2	106.3	244.1	93.3	1a
G	29.0	0.1	452.0	61.9	-1.1	108.1	239.9	87.3	1a
H	35.1	0.1	451.6	69.4	-0.5	125.6	241.7	102.6	1a
I	39.8	0.1	461.4	66.1	-17.1	117.4	237.5	89.2	1a
J	44.2	0.1	455.9	54.4	-10.5	88.5	247.2	70.3	1a
K	50.5	0.2	373.3	70.9	93.3	120.1	279.8	100.0	1b
L	55.0	0.4	444.3	40.6	12.8	74.3	246.6	60.3	1a
M	60.1	0.4	438.6	47.3	22.7	86.1	254.2	77.1	1a
N	65.1	0.4	435.5	62.3	26.9	102.8	257.7	44.0	1a

^aThe expanded uncertainty (U) shows the combined standard uncertainty with a coverage factor of 2, corresponding to a level of confidence of approximately 95%.

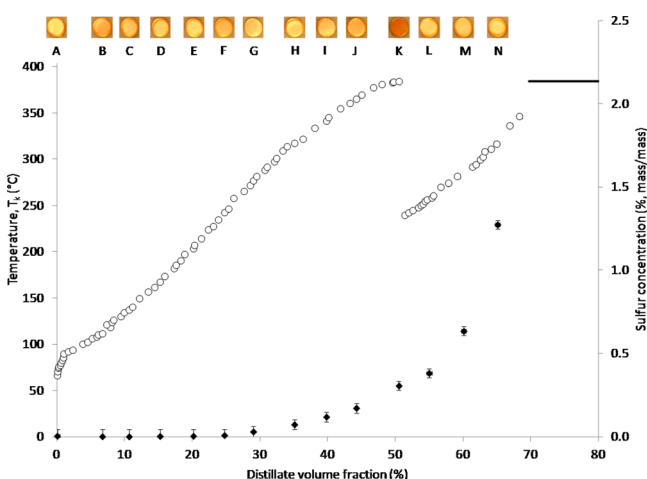


Figure 12. Single distillation curve data for a composite North American crude oil sample at 83.1 kPa (with an expanded uncertainty of 0.7 kPa) and 1.1 kPa (with an expanded uncertainty of 0.7 kPa), plotted as open circles (O). Corresponding mass concentrations of sulfur are plotted as a function of distillate volume fraction (%) on the secondary y-axis. Sulfur concentration of the residue fraction is shown as a solid line from 70% to 80% (volume/volume). Image data of copper corrosivity specimen are shown along the secondary x-axis and correspond to the sulfur concentration values. Table 8 lists $L^*a^*b^*$ values for the copper disks shown. The error bars based on the expanded uncertainties in the measurement are typically smaller than the plotting symbols used in the figure.

This work is significant in illustrating the applicability of the combined ambient-reduced pressure ADC approach to petroleomics by providing the thermophysical and chemical data needed to model some properties of petroleum based on its composition. Furthermore, it demonstrates that GC-MS compositional data coupled with critically evaluated thermodynamic data can be used to estimate fluid properties such as density and refractive index. In addition, it presents evidence that sulfur content alone is insufficient in predicting corrosion. The data presented in Tables 1, 4, and 6 may be useful in the development or refinement of equation of state models for petroleum. Lastly, vector-based image analysis of corrosion samples in $L^*a^*b^*$ color space provides an algorithmic

approach to sample classification based on image data, reducing the variability due to differences in human color perception.

■ ASSOCIATED CONTENT

📄 Supporting Information

Figures S1–S3, Tables S1–S4, text, and references. This material is available free of charge via the Internet at <http://pubs.acs.org>.

■ AUTHOR INFORMATION

Corresponding Author

*Phone: 1-303-497-5158. Fax: 1-303-497-5044. E-mail: bruno@boulder.nist.gov.

Notes

The authors declare no competing financial interest.

■ ACKNOWLEDGMENTS

This research was performed while Peter Y. Hsieh held a National Research Council Research Associateship Award at NIST. We acknowledge the assistance of an oil company in providing the petroleum sample used in this study. For reasons of corporate confidentiality, we are unable to provide additional identifying information on the source of the crude oil. We acknowledge Dr. Katherine P. Rice at NIST for performing the X-ray energy dispersive spectroscopy measurements and analysis.

■ ABBREVIATIONS AND ACRONYMS

a^* = red-green color-opponent axis

ADC = Advanced Distillation Curve

ASTM = ASTM International (formerly American Society for Testing and Materials)

b^* = yellow-blue color-opponent axis

CCD = charge-coupled device

GC-FID = gas chromatography with flame ionization detection

GC-MS = gas chromatography with mass spectrometric detection

GC-SCD = gas chromatography with sulfur chemiluminescence detection

IBT = initial boiling temperature

I^T = programmed-temperature retention index
 L^* = lightness axis
 M = molecular mass
nD20 = refractive index at 589 nm and 20 °C
NIST = National Institute of Standards and Technology
PID = proportional, integral, derivative
QSPR = quantitative structure property relationship
SRM = standard reference material
 T_h = headspace temperature
 T_k = fluid temperature
 U = expanded uncertainty
 V = volume; distillate volume fraction (% volume/volume)
 u_c = combined standard uncertainty
TRC = Thermodynamics Research Center
UCM = unresolved complex mixture
 ρ_d = distillate fraction density
 ρ_r = residue fraction density

REFERENCES

- (1) Rodgers, R. P.; Schaub, T. M.; Marshall, A. G. *Anal. Chem.* **2005**, *77*, 20 A..
- (2) Marshall, A. G.; Rodgers, R. P. *Proc. Natl. Acad. Sci.* **2008**, *105*, 18090.
- (3) Heavy-Duty Engine and Vehicle Standards and Highway Diesel Fuel Sulfur Control Requirements 2000, Regulatory Announcement EPA420-F-00-057, U.S. Environmental Protection Agency: 2000.
- (4) Commission Directive 2006/51/EC, *Official Journal of the European Union* **2006**, L 152/11 - L 152/21.
- (5) Commission Regulation (EU) 582/2011, *Official Journal of the European Union* **2011**, L 167/1 - L 167/168.
- (6) Bartholomew, C. H. *Appl. Catal., A* **2001**, *212*, 17.
- (7) Gary, J. H.; Handwerk, G. E. *Petroleum Refining*; Marcel Dekker: New York, 1975.
- (8) Kabe, T.; Ishihara, A.; Qian, W. *Hydrodesulfurization and Hydrodenitrogenation*; Wiley-VCH: New York, 1999.
- (9) Schulz, H.; Bohringer, W.; Ousmanov, F.; Waller, P. *Fuel Process. Technol.* **1999**, *61*, 5.
- (10) Sanders, J. M. *J. Chem. Soc.* **1912**, *101*, 358.
- (11) Christie, A. W.; Bisson, C. S. *J. Ind. Eng. Chem. (Washington, D. C.)* **1920**, *12*, 171.
- (12) Bjerregaard, A. P. *Ind. Eng. Chem.* **1925**, *17*, 142.
- (13) Harrison, S.; Harvey, D. *Analyst* **1954**, *79*, 640.
- (14) Martin, R. L.; Grant, J. A. *Anal. Chem.* **1965**, *37*, 644.
- (15) Drushel, H. V. *Anal. Chem.* **1978**, *50*, 76.
- (16) Alder, J. F.; Kargosha, K. *Anal. Chim. Acta* **1979**, *111*, 145.
- (17) Akimoto, H.; Finlayson, B. J.; Pitts, J. N. *Chem. Phys. Lett.* **1971**, *12*, 199.
- (18) Benner, R. L.; Stedman, D. H. *Anal. Chem.* **1989**, *61*, 1268.
- (19) Gorbaty, M. L.; George, G. N.; Kelemen, S. R. *Fuel* **1990**, *69*, 945.
- (20) Kelemen, S. R.; George, G. N.; Gorbaty, M. L. *Fuel* **1990**, *69*, 939.
- (21) Waldo, G. S.; Mullins, O. C.; Pennerhahn, J. E.; Cramer, S. P. *Fuel* **1992**, *71*, 53.
- (22) Riazi, M. R.; Nasimi, N.; Roomi, Y. A. *Ind. Eng. Chem. Res.* **1999**, *38*, 4507.
- (23) Standard test method for distillation of petroleum products at atmospheric pressure, ASTM Standard D86-12, *Book of Standards*; ASTM: West Conshohocken, PA, 2012.
- (24) Standard test method for density, relative density, and API gravity of liquids by digital density meter, ASTM Standard D4052-11, *Book of Standards*; ASTM: West Conshohocken, PA, 2011.
- (25) Standard test method for refractive index and refractive dispersion of hydrocarbon liquids, ASTM Standard D1218-12, *Book of Standards*; ASTM: West Conshohocken, PA, 2012.
- (26) Bruno, T. J.; Ott, L. S.; Smith, B. L.; Lovestead, T. M. *Anal. Chem.* **2010**, *82*, 777.
- (27) Bruno, T. J.; Ott, L. S.; Lovestead, T. M.; Huber, M. L. *Chem. Eng. Technol.* **2010**, *33*, 363.
- (28) Bruno, T. J.; Ott, L. S.; Lovestead, T. M.; Huber, M. L. *J. Chromatogr. A* **2010**, *1217*, 2703.
- (29) Bruno, T. J. *Ind. Eng. Chem. Res.* **2006**, *45*, 4371.
- (30) Hadler, A. B.; Ott, L. S.; Bruno, T. J. *Fluid Phase Equilib.* **2009**, *281*, 49.
- (31) Bruno, T. J.; Smith, B. L. *Ind. Eng. Chem. Res.* **2006**, *45*, 4381.
- (32) Smith, B. L.; Bruno, T. J. *Energy Fuels* **2007**, *21*, 2853.
- (33) Smith, B. L.; Bruno, T. J. *Ind. Eng. Chem. Res.* **2007**, *46*, 310.
- (34) Smith, B. L.; Bruno, T. J. *J. Propul. Power* **2008**, *24*, 618.
- (35) Bruno, T. J.; Baibourine, E.; Lovestead, T. M. *Energy Fuels* **2010**, *24*, 3049.
- (36) Burger, J. L.; Bruno, T. J. *Energy Fuels* **2012**, *26*, 3661.
- (37) Ott, L. S.; Bruno, T. J. *Energy Fuels* **2008**, *22*, 2861.
- (38) Smith, B. L.; Ott, L. S.; Bruno, T. J. *Environ. Sci. Technol.* **2008**, *42*, 7682.
- (39) Smith, B. L.; Ott, L. S.; Bruno, T. J. *Ind. Eng. Chem. Res.* **2008**, *47*, 5832.
- (40) Bruno, T. J.; Wolk, A.; Naydich, A.; Huber, M. L. *Energy Fuels* **2009**, *23*, 3989.
- (41) Windom, B. C.; Lovestead, T. M.; Mascal, M.; Nikitin, E. B.; Bruno, T. J. *Energy Fuels* **2011**, *25*, 1878.
- (42) Hsieh, P. Y.; Abel, K. R.; Bruno, T. J. *Energy Fuels* **2013**, *27*, 804.
- (43) Smith, B. L.; Bruno, T. J. *Ind. Eng. Chem. Res.* **2007**, *46*, 297.
- (44) Bruno, T. J.; Wolk, A.; Naydich, A. *Energy Fuels* **2009**, *23*, 2295.
- (45) Bruno, T. J.; Wolk, A.; Naydich, A. *Energy Fuels* **2009**, *23*, 3277.
- (46) Ott, L. S.; Hadler, A. B.; Bruno, T. J. *Ind. Eng. Chem. Res.* **2008**, *47*, 9225.
- (47) Lovestead, T. M.; Bruno, T. J. *Energy Fuels* **2009**, *23*, 3637.
- (48) Lovestead, T. M.; Windom, B. C.; Riggs, J. R.; Nickell, C.; Bruno, T. J. *Energy Fuels* **2010**, *24*, 5611.
- (49) Ott, L. S.; Bruno, T. J. *Energy Fuels* **2007**, *21*, 2778.
- (50) Ott, L. S.; Bruno, T. J. *J. Sulfur Chem.* **2007**, *28*, 493.
- (51) Ott, L. S.; Smith, B. L.; Bruno, T. J. *Fuel* **2008**, *87*, 3379.
- (52) Ott, L. S.; Smith, B. L.; Bruno, T. J. *Fuel* **2008**, *87*, 3055.
- (53) Huber, M. L.; Smith, B. L.; Ott, L. S.; Bruno, T. J. *Energy Fuels* **2008**, *22*, 1104.
- (54) Huber, M. L.; Lemmon, E. W.; Diky, V.; Smith, B. L.; Bruno, T. J. *Energy Fuels* **2008**, *22*, 3249.
- (55) Huber, A. L.; Lemmon, E. W.; Ott, L. S.; Bruno, T. J. *Energy Fuels* **2009**, *23*, 3083.
- (56) Bruno, T. J.; Huber, M. L. *Energy Fuels* **2010**, *24*, 4277.
- (57) Huber, M. L.; Lemmon, E. W.; Bruno, T. J. *Energy Fuels* **2010**, *24*, 3565.
- (58) Mueller, C. J.; Cannella, W. J.; Bruno, T. J.; Bunting, B.; Dettman, H. D.; Franz, J. A.; Huber, M. L.; Natarajan, M.; Pitz, W. J.; Ratcliff, M. A.; Wright, K. *Energy Fuels* **2012**, *26*, 3284.
- (59) Andersen, W. C.; Abdulagatov, A. I.; Bruno, T. J. *Energy Fuels* **2003**, *17*, 120.
- (60) Garverick, L. *Corrosion in the Petrochemical Industry*; ASM International: 1994.
- (61) Windom, B. University of Colorado, Colorado Springs, CO, *Personal communication*, 2013.
- (62) Windom, B. C.; Bruno, T. J. *J. Chromatogr. A* **2010**, *1217*, 7434.
- (63) Windom, B. C.; Bruno, T. J. *Ind. Eng. Chem. Res.* **2011**, *50*, 1115.
- (64) Windom, B. C.; Bruno, T. J. *Ind. Eng. Chem. Res.* **2013**, *52*, 327.
- (65) Riazi, M. R. *Characterization and Properties of Petroleum Fractions*; ASTM International: West Conshohocken, PA, 2005.
- (66) Maxwell, J. B.; Bonnell, L. S. *Vapor Pressure Charts for Petroleum Engineers*; Esso Research and Engineering Company: 1955.
- (67) Bruno, T. J.; Svoronos, P. D. N. *Handbook of Basic Tables for Chemical Analysis*, 3rd ed.; Taylor & Francis: Boca Raton, FL, 2011.
- (68) Stein, S. E.; Babushok, V. I.; Brown, R. L.; Linstrom, P. J. *J. Chem. Inf. Model.* **2007**, *47*, 975.
- (69) Kitamaki, Y.; Shimizu, Y.; Kato, K. *Anal. Bioanal. Chem.* **2008**, *391*, 2089.

- (70) Standard test method for copper strip corrosion by liquefied petroleum (LP) gases, ASTM Standard D1838-12, *Book of Standards*; ASTM: West Conshohocken, PA, 2012.
- (71) Schneider, C. A.; Rasband, W. S.; Eliceiri, K. W. *Nat. Methods* **2012**, *9*, 671.
- (72) Barilla, M. E. *Color Transformer plug-in*; Birmingham, UK, 2013.
- (73) Taylor, B. N.; Kuyatt, C. E. *Guidelines for evaluating and expressing the uncertainty of NIST measurement results*; NIST: 1994.
- (74) Gamble, L. W.; Jones, W. H. *Anal. Chem.* **1955**, *27*, 1456.
- (75) Heberger, K. J. *Chromatogr. A* **2007**, *1158*, 273.
- (76) Gonzalez, F. R.; Nardillo, A. M. J. *Chromatogr. A* **1999**, *842*, 29.
- (77) Sanchez, I. C.; Lacombe, R. H. *J. Phys. Chem.* **1976**, *80*, 2352.
- (78) Katritzky, A. R.; Ignatchenko, E. S.; Barcock, R. A.; Lobanov, V. S.; Karelson, M. *Anal. Chem.* **1994**, *66*, 1799.
- (79) Kazakov, A. F.; Muzny, C. D.; Chirico, R. D.; Diky, V.; Frenkel, M.; 2-2012-1-Pro ed.; Standard Reference Data Program: Gaithersburg, MD, 2012.
- (80) Diky, V.; Muzny, C. D.; Lemmon, E. W.; Chirico, R. D.; Frenkel, M. *J. Chem. Inf. Model.* **2007**, *47*, 1713.
- (81) Harrison, C.; Winnick, J. *J. Chem. Eng. Data* **1967**, *12*, 176.
- (82) Bhattacharyya, S. N.; Patterson, D. J. *Chem. Soc., Faraday Trans. 1* **1985**, *81*, 375.
- (83) Cheng, H. M.; Liu, M.; Shen, Z. H.; Xi, J. Z.; Sano, H.; Uchiyama, Y.; Kobayashi, K. *Carbon* **1997**, *35*, 869.
- (84) *CRC Handbook of Chemistry and Physics*, 93rd ed.; Haynes, W. M.; Lide, D. R.; Bruno, T. J., Eds.; CRC Press: 2012.
- (85) Riazi, M. R.; Daubert, T. E. *Ind. Eng. Chem. Res.* **1987**, *26*, 755.
- (86) Speight, J. G.; Moschopedis, S. E. *Adv. Chem. Ser.* **1981**, *195*, 1.